



HHF
9,8

860

Received February 1999
Revised June 1999
Accepted July 1999

An explicit finite element algorithm for convection heat transfer problems

M.T. Manzari

*Department of Mechanical Engineering, University of Wales, Swansea,
Wales, UK*

Keywords *Explicit method, Finite element, Laminar flow, Convection, Heat transfer*

Abstract *A finite element algorithm is presented for the simulation of steady incompressible fluid flow with heat transfer using triangular meshes. The continuity equation is modified by employing the artificial compressibility concept to provide coupling between the pressure and velocity fields of the fluid. A standard Galerkin finite element method is used for spatial discretization and an explicit multistage Runge-Kutta scheme is used to march in the time domain. The resulting procedure is stabilized using an artificial dissipation technique. To demonstrate the performance of the proposed algorithm a wide range of test cases is solved including applications with and without heat transfer. Both natural and forced convection applications are studied.*

Introduction

Numerical simulation of convection heat transfer in incompressible fluid flows is of great practical importance due to their numerous applications in many industrial devices such as heat exchangers, cooling of electronic systems, etc. The diversity of flow regimes and heat transfer rates in different applications emphasizes the need for a generalized simulation method which can handle most flow conditions without *ad hoc* modifications. The flow characteristics in convection heat transfer are normally identified using three parameters; Reynolds number, Prandtl number and Grashof number. The Reynolds number controls the flow domain and specifies the limit of laminar flow regime and the size of recirculation zones, etc. The Prandtl number, on the other hand, controls the temperature field and its relationship with the flow characteristics. When natural convection is present, the buoyancy force also becomes the driving force for both fluid flow and heat transfer phenomena, and the Grashof number is important.

In the context of incompressible fluid flow, two different approaches are normally adopted to satisfy the incompressibility constraint and couple the pressure and velocity fields:

- (1) pressure based methods;
- (2) artificial compressibility (AC) methods.

Tamamidis *et al.* (1996) provide a comparative study of the two methods. The AC method, which is adopted in this paper, is especially suitable for use in conjunction with a compressible flow solver. The concept of artificial compressibility was first introduced by Chorin (1967) and extensively used by

other researchers since. In this method, a pseudo-temporal pressure term is added to the continuity equation to impose the incompressibility constraint. As a result, the high speed sound waves are eliminated and the modified system becomes much better conditioned for numerical solution. The original version of the AC method is only accurate for the steady state problems; however; Wasfy *et al.* (1998) have recently shown that the method can be extended to solve the unsteady flow problems. Various types of the upwind and artificial dissipation schemes have been used in conjunction with AC to provide stable numerical methods. Lin and Sotiropoulos (1997) have compared three different numerical dissipation techniques and reported their merits and deficiencies. In this work, an artificial dissipation method (AD) due to Jameson *et al.* (1981) is adopted. This method is especially popular among CFD practitioners because of its simplicity and computational efficiency.

Both the AC and AD methods have already been used in many fields of fluid dynamics. However, in the context of finite element method, their use had been limited to the isothermal problems. Manzari *et al.* (1998) have recently developed an AD-based algorithm for 3D compressible turbulent flow problems and shown that it performs well for a wide range of flow regimes. They have also shown that by employing parallel computing techniques the efficiency of the method can be greatly enhanced (Manzari *et al.*, 1998). These promising achievements encouraged the author to extend the scheme to the incompressible flow problems with heat transfer. At this stage only laminar flow problems are considered. In this paper, first the modified system of governing equations for incompressible viscous flow with heat transfer is presented and the associated initial and boundary conditions are described. Then, the numerical solution procedure including the spatial and temporal discretizations is elaborated. Finally, a number of problems with and without heat transfer are solved, and the accuracy and suitability of the proposed method are examined.

Governing equations

A complete set of equations to describe laminar flow of an incompressible fluid with heat transfer consists of equations for conservation of mass, momentum and energy. Assuming a Newtonian fluid with negligible viscous dissipation, the governing system of equations in a Cartesian coordinate system Ox_1x_2 can be written in the non-dimensional conservation form as

$$\frac{\partial \mathbf{U}}{\partial t} + \frac{\partial \mathbf{F}^j}{\partial x_j} = \frac{\partial \mathbf{G}^j}{\partial x_j} + \mathbf{S}, \quad j = 1, 2 \quad (1)$$

where

$$\mathbf{U} = \begin{bmatrix} p \\ u_1 \\ u_2 \\ T \end{bmatrix} \quad \mathbf{F}^j = \begin{bmatrix} \beta^2 u_j \\ u_1 u_j + p \delta_{1j} \\ u_2 u_j + p \delta_{2j} \\ T u_j \end{bmatrix} \quad \mathbf{G}^j = \begin{bmatrix} 0 \\ \tau_{1j} \\ \tau_{2j} \\ \frac{1}{Pe} \frac{\partial T}{\partial x_j} \end{bmatrix} \quad \mathbf{S} = \begin{bmatrix} 0 \\ 0 \\ \frac{Gr}{Re^2} T \\ 0 \end{bmatrix} \quad (2)$$

In these equations, t denotes time, u_i is the velocity in direction x_i , p is pressure, T is temperature, β^2 is a constant and δ_{ij} is the Kronecker delta. In addition Reynolds number, Peclet number and Grashof number are defined as

$$Re = \frac{\rho_0^* U^* L^*}{\mu_0^*} \quad Pe = RePr \quad Gr = \frac{L^{*3} \rho_0^{*2} g (\beta_T \Delta T)}{\mu_0^{*2}} \quad (3)$$

where L^* and U^* are the characteristic length and velocity used for non-dimensionalization, μ_0^* is the molecular dynamic viscosity at a reference temperature T_0^* and Pr is the Prandtl number. Also, the stress tensor τ_{ij} is defined as

$$\tau_{ij} = \frac{\mu}{Re} \left(\frac{\partial u_i}{\partial x_j} + \frac{\partial u_j}{\partial x_i} \right) \quad (4)$$

The non-dimensional quantities are related to their dimensional counterparts (indicated here by superscript $*$) via the following relations

$$t = \frac{t^* U^*}{L^*} \quad u_i = \frac{u_i^*}{U^*} \quad p = \frac{p^*}{\rho_0^* U^{*2}} \quad T = \frac{T^* - T_0^*}{T_w^* - T_0^*} \quad \mu = \frac{\mu^*}{\mu_0^*} \quad (5)$$

where ρ_0^* is the fluid density at T_0^* and T_w^* is the wall temperature. In external flow problems, freestream values are chosen for U^* and T_0^* , whilst in duct flow problems the flow entrance condition is used for this purpose. As was mentioned earlier and will be noticed from equation (2), the continuity equation has been written in a modified form with an extra transient term. This form enables us to solve incompressible flow problems using the compressible flow solvers. The artificial transient term $\frac{\partial p}{\partial t}$ helps to eliminate the high speed sound waves associated with the system. The parameter β^2 is a constant which is selected to accelerate convergence to the steady state solution. β^2 can be related to the local Mach number in compressible flows and following Rizzi and Eriksson (1984), we use $\beta^2 = \max(0.3, ru_i u_i)$ with $1 < r < 5$. It must be emphasized here that although the system of equations (1) has no physical meaning as it stands, it represents exactly our physical problem when the steady state condition is reached.

In equation (2) it is assumed that the gravity force is in the y direction and therefore the buoyancy force in natural convection acts in the y direction only. If in a problem natural convection is negligible, Gr is set to zero. For isothermal flow problems, the energy equation is omitted from the system of equations and only the first three equations in equation (1) are solved.

Initial and boundary conditions

Let us consider a domain, Ω , which is bounded by a closed surface, Γ , with unit outward normal vector $\mathbf{n} = (n_1, n_2)$. A complete definition of the above problem requires the definition of an appropriate set of initial and boundary conditions. Two types of problems are considered; isothermal

and non-isothermal. For non-isothermal problems only, a set of initial and boundary conditions are required for temperature. In such problems, the initial temperature is set to zero and two types of boundary conditions are considered; isothermal wall and adiabatic wall. In the case of an isothermal wall, temperatures everywhere on the wall are set to a prescribed value. For an adiabatic wall no heat transfer is allowed through the boundary.

Both isothermal and non-isothermal problems, however, require initial and boundary conditions for the pressure and velocity fields. Again two types of flow domains are possible; external and internal flows. For external flows, the freestream values are imposed everywhere in Ω as initial conditions whilst for internal flows the entrance conditions are used for this purpose.

At the entrance section of an internal (channel) flow or at the inflow boundary of an external flow, only flow velocities are imposed and the pressure field is computed. At the exit section of an internal flow or at the outflow boundary of an external flow, the pressure field is set to zero and the velocity field is computed.

At a wall boundary, the no slip condition $u_i = 0$ is imposed. For a symmetric boundary, an adiabatic boundary is assumed for the temperature field and the slip condition is imposed for the velocity field by cancelling the normal component of the velocity vector.

Solution algorithm

Spatial discretization

The first stage for solving the problem in hand by the finite element method is to transform it into a weak variational form. This weak form can be written as: find \mathbf{U} such that

$$\int_{\Omega} \frac{\partial \mathbf{U}}{\partial t} W d\Omega = \int_{\Omega} \mathbf{F}^j \frac{\partial W}{\partial x_j} d\Omega - \int_{\Gamma} \bar{\mathbf{F}}^j n_j W d\Gamma - \int_{\Omega} \mathbf{G}^j \frac{\partial W}{\partial x_j} d\Omega + \int_{\Gamma} \bar{\mathbf{G}}^j n_j W d\Gamma + \int_{\Omega} \mathbf{S} W d\Omega \quad (6)$$

for all suitable weighting functions, W , and for all $t > t_0$. In this expression, an overbar represents a prescribed normal boundary flux.

Next the solution domain Ω is discretized using triangular elements, with nodes numbered $1, \dots, P$ located at the element vertices. A piecewise linear approximate solution is assumed in the form

$$\mathbf{U} \approx \mathbf{U}^{(P)} = \mathbf{U}_J(t) N_J(\mathbf{x}) \quad J = 1, \dots, P \quad (7)$$

where N_J represents the linear finite element shape function associated with node J and \mathbf{U}_J is the value of the approximation at node J . A Galerkin approximate solution is produced using the variational formulation of the problem in the form: find $\mathbf{U}^{(P)}$ such that

$$\int_{\Omega} \frac{\partial \mathbf{U}^{(P)}}{\partial t} N_I d\Omega = \int_{\Omega} \mathbf{F}^{j(P)} \frac{\partial N_I}{\partial x_j} d\Omega - \int_{\Gamma} \bar{\mathbf{F}}^{j(P)} n_j N_I d\Gamma \quad (8)$$

$$- \int_{\Omega} \mathbf{G}^{j(P)} \frac{\partial N_I}{\partial x_j} d\Omega + \int_{\Gamma} \bar{\mathbf{G}}^{j(P)} n_j N_I d\Gamma + \int_{\Omega} \mathbf{S}^{(P)} N_I d\Omega$$

for $I = 1, 2, \dots, P$ and for all $t > t_0$. The integrals appearing in this Galerkin statement are evaluated, using an edge-based data structure (Peraire *et al.*, 1993), in the form

$$\left[\mathbf{M} \frac{d\mathbf{U}}{dt} \right]_I = - \sum_{s=1}^{m_I} \frac{C_{I_s}^j}{2} \{ (\mathbf{F}_I^j + \mathbf{F}_{I_s}^j) - (\mathbf{G}_I^j + \mathbf{G}_{I_s}^j) \} + [\mathbf{M}_L]_I \mathbf{S}_I$$

$$+ \left\langle \sum_{f=1}^2 D_f \{ (4\bar{\mathbf{F}}_I^n + 2\bar{\mathbf{F}}_{J_f}^n + \mathbf{F}_I^n - \mathbf{F}_{J_f}^n) \right.$$

$$\left. - (4\bar{\mathbf{G}}_I^n + 2\bar{\mathbf{G}}_{J_f}^n + \mathbf{G}_I^n - \mathbf{G}_{J_f}^n) \right\rangle_I \quad (9)$$

where the edge s in the mesh joins nodes I and I_s , and J_1 and J_2 are the boundary nodes which are connected to the boundary node I . Note that the terms $\langle \cdot \rangle_I$ are only non-zero when node I is a boundary node. The weights $C_{I_s}^j$ and D_f are computed as

$$C_{I_s}^j = - \sum_{E \in I_s} \frac{2\Omega_E}{3} \left[\frac{\partial N_I}{\partial x_j} \right]_E + \left\langle \sum_{f \in I_s} \frac{\Gamma_f}{6} n_j \right\rangle \quad D_f = - \frac{\Gamma_f}{12} \quad (10)$$

where Ω_E is the surface area of the element E and n_j is the component in the x_j direction of the unit normal to the boundary edge f , of length Γ_f , which joins the nodes I and J_f . An advantage of this edge data structure is that it leads to savings in both CPU and memory requirements especially when 3D simulations are attempted (Peraire *et al.*, 1993). For the steady flow analysis which is of interest here, the consistent finite element mass matrix \mathbf{M} which appears in equation (9) is replaced by the diagonal lumped mass matrix \mathbf{M}_L . The nodal values of the gradients of \mathbf{U} , which are required before the viscous fluxes \mathbf{G}_I^j can be evaluated for use in equation (9), are also obtained in a variational form (Lyra *et al.*, 1995) as

$$\left[\mathbf{M}_L \frac{\partial \mathbf{U}}{\partial x_j} \right]_I = \sum_{s=1}^{m_I} \frac{C_{I_s}^j}{2} (\mathbf{U}_I + \mathbf{U}_{I_s}) - \left\langle \sum_{f=1}^2 D_f n_j (5\mathbf{U}_I + \mathbf{U}_{J_f}) \right\rangle_I \quad (11)$$

The semi-discrete finite element formulation (9) represents a central difference type of approximation to the spatial derivatives and is prone to produce spurious oscillations which can cause numerical instabilities. Therefore, a form of stabilization will be required before it can be used for the simulation of flow problems. This is discussed next.

Stabilization technique

In this work, an artificial dissipation scheme due to Jameson *et al.* (1981) is used to stabilize the solution procedure. This scheme is a simple yet computationally efficient method in which a background diffusion term is added to the right-hand side of equation (9). The diffusion \mathbf{D}_I added at a general node I is constructed as a fourth order operator in the form of

$$\mathbf{D}_I = - \sum_{s=1}^{m_I} \epsilon_{II_s}^{(4)} (\nabla^2 \mathbf{U}_{I_s} - \nabla^2 \mathbf{U}_I) \frac{\min(\lambda_I, \lambda_{I_s})}{m_I + m_{I_s}} \quad (12)$$

where the second order operator is approximated according to

$$\nabla^2 \mathbf{U}_I \approx \frac{1}{m_I} \sum_{s=1}^{m_I} (\mathbf{U}_{I_s} - \mathbf{U}_I) \quad (13)$$

Here m_I denotes the number of edges connected to the node I and λ is the maximum eigenvalue of the Jacobian matrix $l_j \partial \mathbf{F}^j / \partial \mathbf{U}$ in absolute value, where $\mathbf{l} = (l_1, l_2)$ is the unit vector in the direction of the edge II_s . The tuning parameter $\epsilon_{II_s}^{(4)}$ is a constant whose value must be optimized for each problem.

Time discretization

A three-stage scheme is employed to advance the solution from time level $t = t_n$ to time level $t = t_{n+1} = t_n + \Delta t$. Within each time step, this scheme is implemented in the form

$$\begin{aligned} \mathbf{U}_I^{(0)} &= \mathbf{U}_I^n \\ \mathbf{U}_I^{(k)} &= \mathbf{U}_I^n - \alpha_k \Delta t [\mathbf{M}_L]^{-1} (\mathbf{R}_I^{(k-1)} - \mathbf{D}_I^{(0)}) \quad \text{for } k = 1, 2, 3 \\ \mathbf{U}_I^{n+1} &= \mathbf{U}_I^{(3)} \end{aligned} \quad (14)$$

Here $\mathbf{R}_I^{(k-1)}$ represents the right-hand side of equation (9) computed at the stage $k - 1$, while the added diffusion \mathbf{D}_I is held constant at the value computed at t^n . The values $\alpha_1 = 0.6$, $\alpha_2 = 0.6$ and $\alpha_3 = 1$ are adopted for the coefficients in equation (14).

In this work, a local time stepping approach is used to accelerate the convergence rate towards the steady-state. The time step used in equation (14) is computed from

$$\Delta t_I = (CFL) [\mathbf{M}]_I \left\{ \sum_{s=1}^{m_I} \left[\mathcal{L}_{II_s} |(\lambda_{\max})_{II_s}| + \frac{2\mathcal{L}_{II_s}^2 \mu_I}{Re[\mathbf{M}]_I} \right] \right\}^{-1} \quad (15)$$

where CFL is the Courant-Friedrichs-Lewy number and the maximum eigenvalue of the Jacobian matrix for edge II_s , is defined as

$$(\lambda_{\max})_{II_s} = |\mathbf{v}_{II_s} \cdot \mathbf{S}_{II_s}| + \beta^2 \quad (16)$$

HFF
9,8

where \mathbf{v}_{II_s} denotes the average velocity of the edge II_s . Here the following notations are used

$$\mathbf{C}_{II_s} = (C_{II_s}^1, C_{II_s}^2) \quad \mathcal{L}_{II_s} = |\mathbf{C}_{II_s}| \quad S_{II_s}^j = \frac{C_{II_s}^j}{|\mathbf{C}_{II_s}|} \quad \mathbf{S}_{II_s} = \frac{\mathbf{C}_{II_s}}{|\mathbf{C}_{II_s}|} \quad (17)$$

866

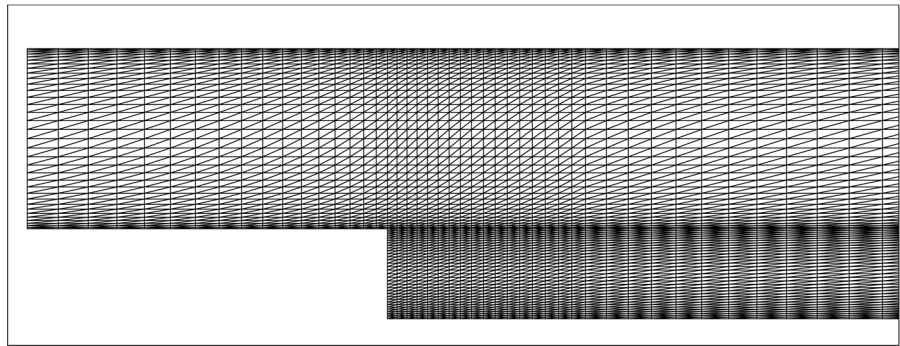
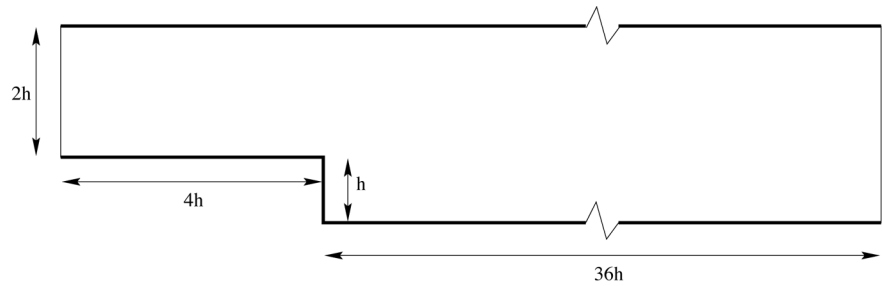


Figure 1.
Flow over a backward facing step ($Re = 229$): schematic of the problem (top) and mesh used (bottom)

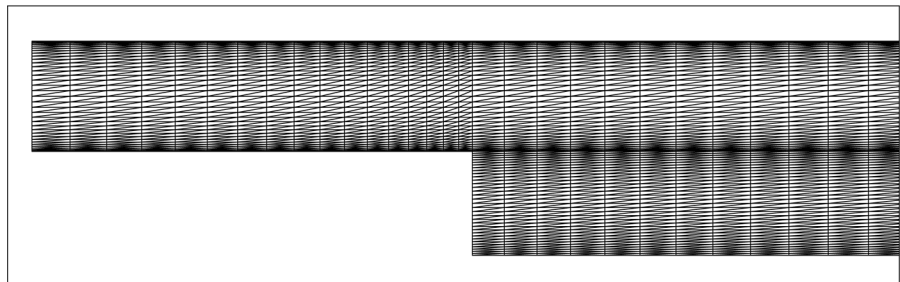
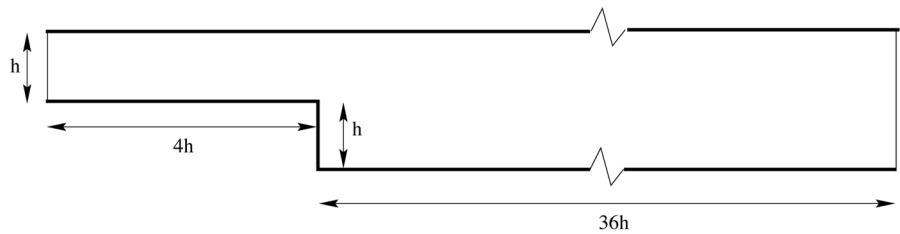


Figure 2.
Flow over a backward facing step ($Re = 389$): schematic of the problem (top) and mesh used (bottom)

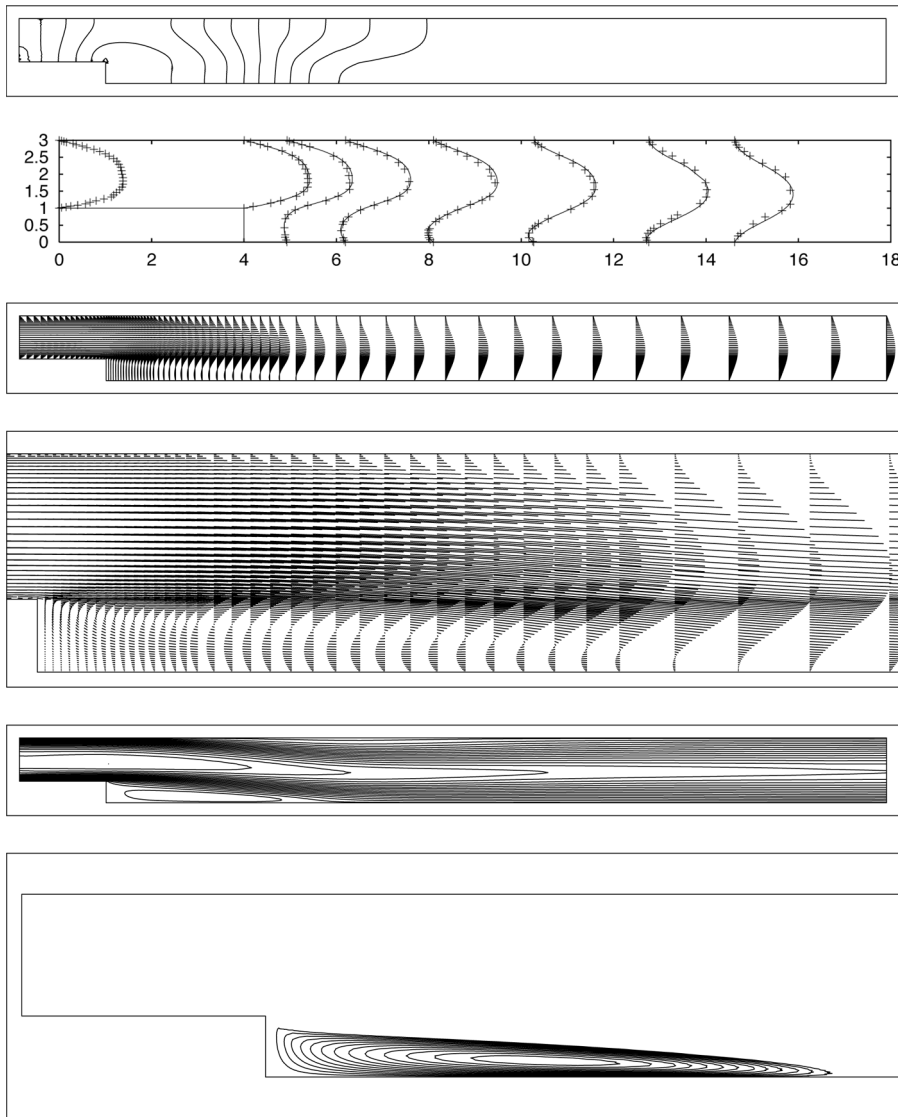


Figure 3.
Flow over a backward
facing step ($Re = 229$):
from top to bottom –
pressure contour plots,
velocity profiles at
different sections
(symbol: experiment,
line: computed), velocity
vectors, velocity vectors
(zoom), and u_1 velocity
contour plot and its
zoom at step

The maximum value of CFL is a function of the flow characteristics and must be optimized for each problem. A value around 0.5 gives satisfactory results for most of the cases solved in this paper but for severe flow conditions such as flows with very high Re numbers, this will need to be decreased an order of magnitude.

Test cases

In this section a number of test cases are solved to examine the performance and accuracy of the proposed scheme. The test cases are chosen from a wide

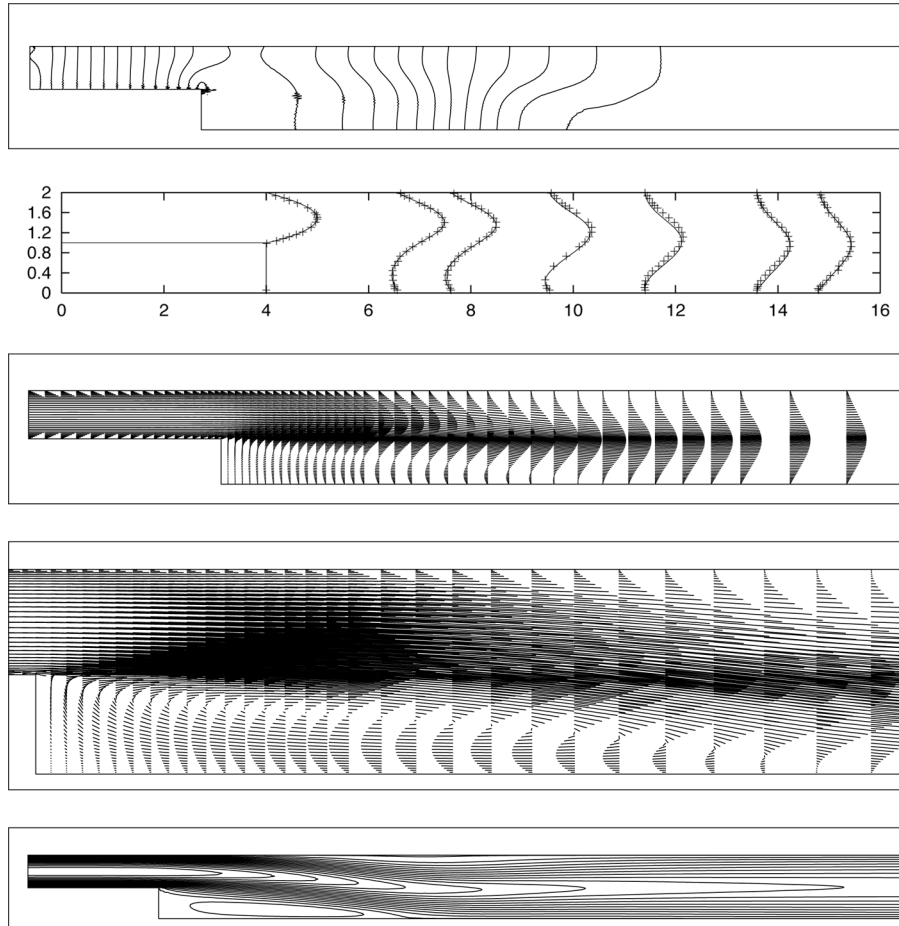


Figure 4. Flow over a backward facing step ($Re = 389$): from top to bottom; pressure contour plots, velocity profiles at different sections (symbol: experiment, line: computed), velocity vectors, velocity contours (zoom), and u_1 velocity contour plot

range of applications to demonstrate the adequacy of the method for solving flow problems without and with heat transfer. The results are compared with experimental or numerical data where available.

Flow over a backward facing step

The first test case is an isothermal flow over a backward facing step. This flow has been extensively used for assessing capabilities of the flow solvers. Both experimental and numerical results are available for various Reynolds numbers. In this paper, two expansion ratios are studied, i.e. 1:2 and 2:3. The experimental data for expansion ratio 1:2 have been given by Armaly *et al.* (1983) and for ratio 2:3 by Denham and Patrick (1974). The Reynolds numbers chosen are 229 and 389 for ratios 2:3 and 1:2, respectively. Figures 1 and 2 show schematics of the flow domains and the meshes used. For both cases a mesh with 4,183 nodes and 8,092 triangular elements is used. The flow downstream of the step is extended for 36

times the height of step to make sure that the outflow is fully developed. Figures 3 and 4 show the result of computations for $Re = 229$ and 389 , respectively. It is seen that for both cases the velocity profiles are in good agreement with the experimental data and quite smooth pressure fields are produced. It must be mentioned that for ratio 1:2, $Re = 389$ is the limit of having a two-dimensional laminar flow. Hence, it can be deduced that the algorithm presented here is capable of solving such problems with a good degree of accuracy. Finally, in Figure 5, the convergence history of L_2 -norm of residuals for three primitive variables (p, u_1, u_2) are shown. These curves show a good convergence behaviour for the proposed method. The computational time for this problem is 50 seconds per 1,000 iterations on a Sun Ultra 1 workstation.

Lid-driven cavity flow

In this test case, a recirculation flow in a square cavity generated by the uniform translation of the upper surface of the cavity (lid) is studied. The speed

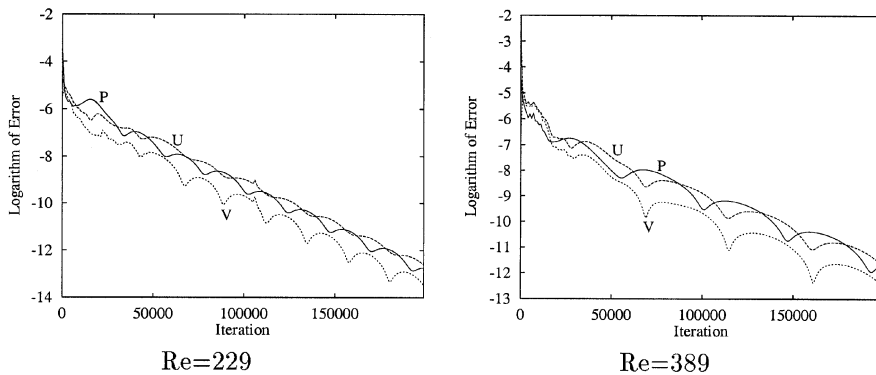


Figure 5.
Flow over a backward
facing step: convergence
history of L_2 -norm of
residuals for primitive
variables (p, u, v)

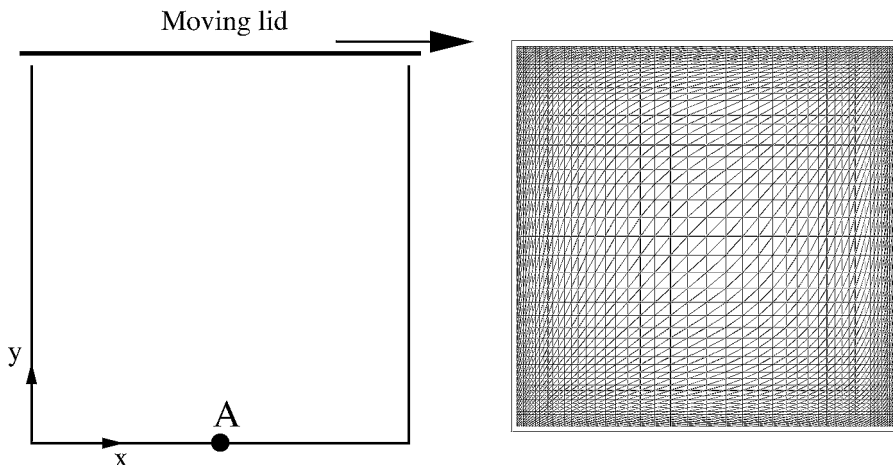
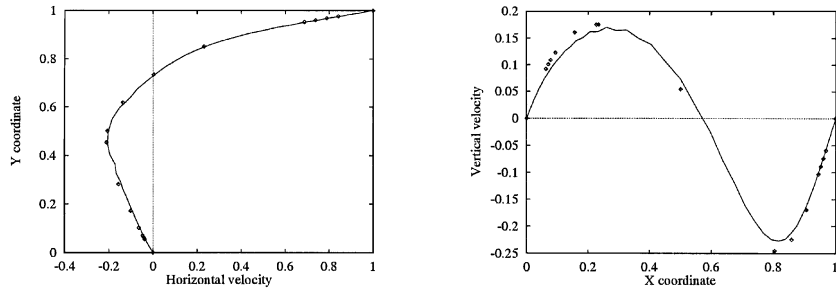
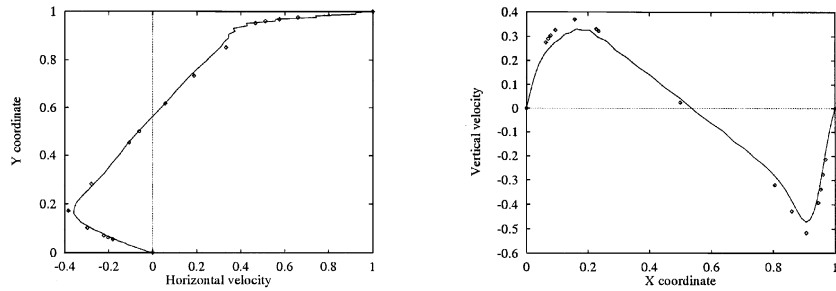


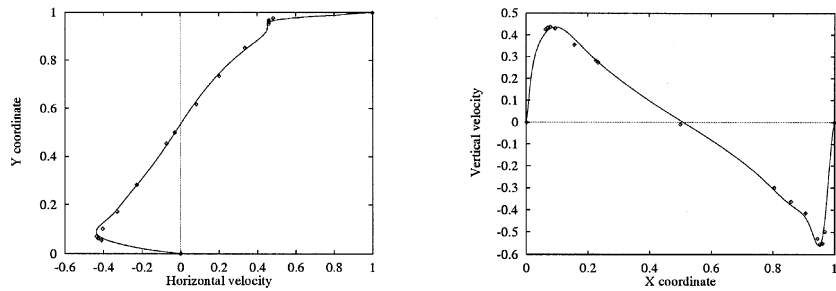
Figure 6.
Lid-driven cavity flow:
schematic of the
problem (left) and mesh
used (right)



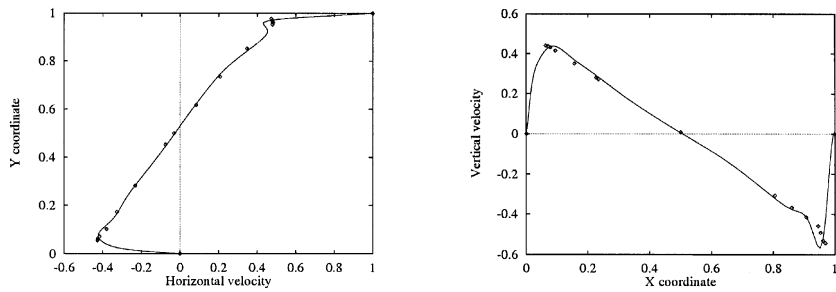
Re=100



Re=1000



Re=5000



Re=10000

Figure 7. Lid-driven cavity flow: velocity profile along $x = 0.5$ (left) and along $y = 0.5$ (right) – line: computed, diamond: experiment

of translation is unity and no fluid can escape from the gap between the cavity and its lid. A schematic of the problem and the mesh used are shown in Figure 6. The mesh consists of 51×51 points and 5,000 triangular elements. In order to define the pressure domain, pressure at point A is set to zero. The problem is solved for $Re = 100, 1,000, 5,000$ and $10,000$. In Figure 7, profiles of the horizontal velocity along the vertical centre line of the cavity and the vertical velocity along the horizontal centre line of the cavity are illustrated for various Reynolds numbers. For comparison, the benchmark solutions obtained by Ghia *et al.* (1982) are also shown in these graphs. It is observed that the computed results are in good agreement with the benchmark solution. As expected from the type of flow solver adopted here, the agreement is even better for higher Reynolds number flows. The largest discrepancy is associated with the vertical velocities which are comparatively small. This is due to the minimum required level of numerical dissipation to maintain the stability of the solution for the mesh spacing used. A finer grid will obviously reduce the discrepancy.

Natural convection in a cavity

In this test case, a pure natural convection in a square cavity is studied. The left and right vertical walls of the cavity are kept at $T = 1$ and $T = 0$, respectively, while the horizontal walls are insulated. Figure 8 shows a schematic of the problem. The computational mesh used is the same as in the previous test case. The Prandtl number is set to unity and the problem is solved for five different Rayleigh numbers; $10^3, 10^4, 10^5, 10^6$ and 10^7 . Figure 9 illustrates a set of plots for each Rayleigh number. These are velocity vectors, u_1 and u_2 contour plots and temperature contours. A comparison with the results presented by de Vahl Davis (1983) shows very good agreements for all cases. Figure 10 shows variations of Nusselt number ($Nu = -\partial T / \partial x$) along the hot and cold walls for various Rayleigh numbers. In Table I, a number of important quantities for this type of flow are presented for various Rayleigh numbers studied here and compared with those given by de Vahl Davis (1983) and Ramaswamy *et al.* (1992). These quantities are the maximum horizontal velocity and its associated y , the maximum vertical velocity and its associated x , the minimum and

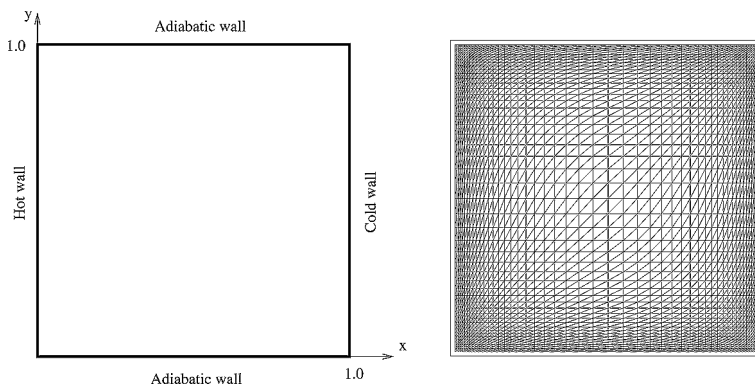


Figure 8.
Natural convection in
cavity: schematic of the
problem (left) and mesh
used (right)

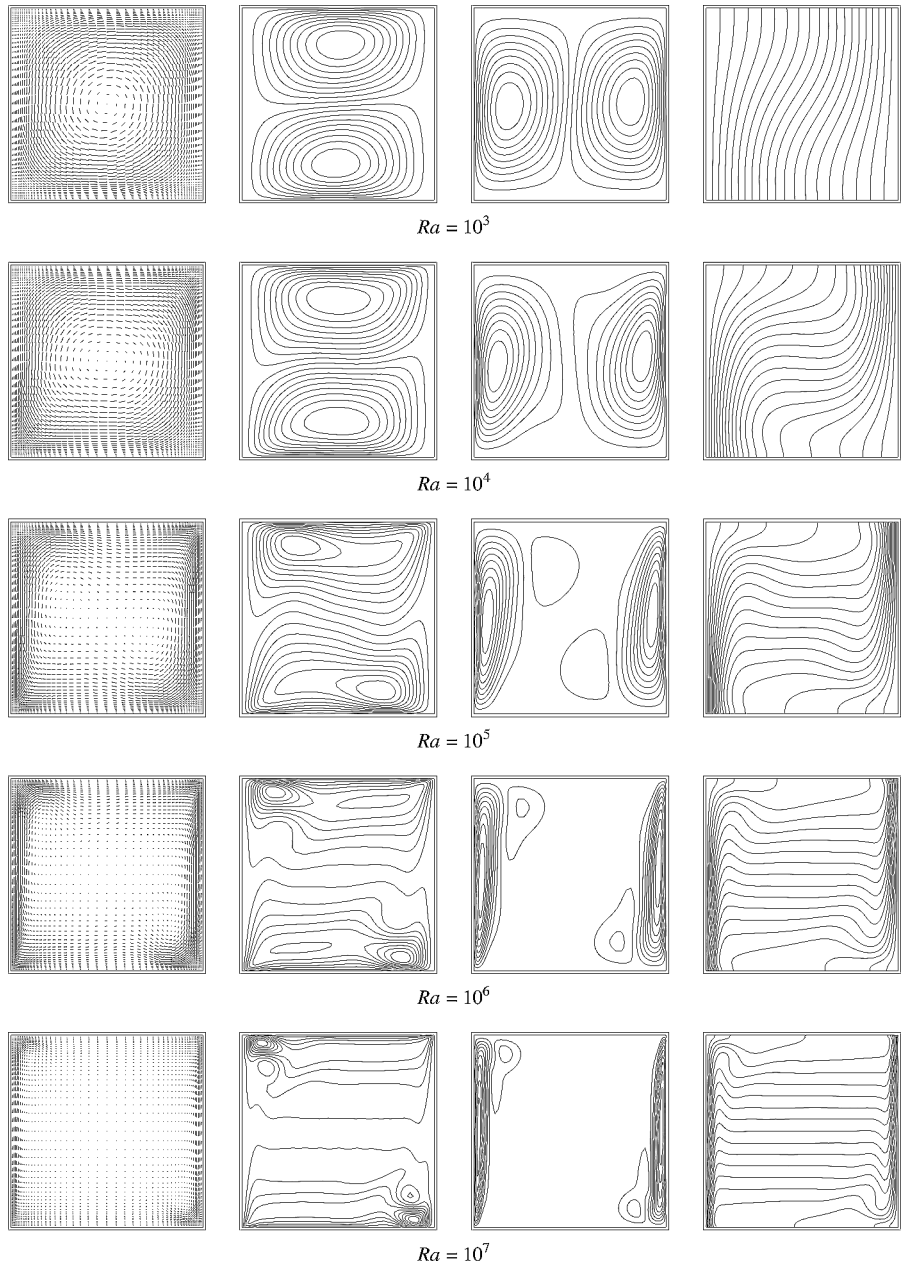


Figure 9. Natural convection in cavity: velocity vectors, u_1 and u_2 velocities and temperature contour plots (left to right)

maximum Nusselt numbers, Nusselt number at $y = 0.5$ and the average Nusselt number. Comparing the computed values with the results obtained by de Vahl Davis (1983) and Ramaswamy *et al.* (1992) shows a close agreement. Finally, the convergence history for the pressure and temperature (for

$Ra = 10^5$) is shown in Figure 11. The convergence history for the velocity components coincide with that of the pressure. Again, as seen for the isothermal flows, these curves demonstrate a good convergence behaviour for the thermal problems as well. The computational time for this problem is 60 seconds per 1,000 iterations on a Sun Ultra 1 workstation.

An explicit finite element algorithm

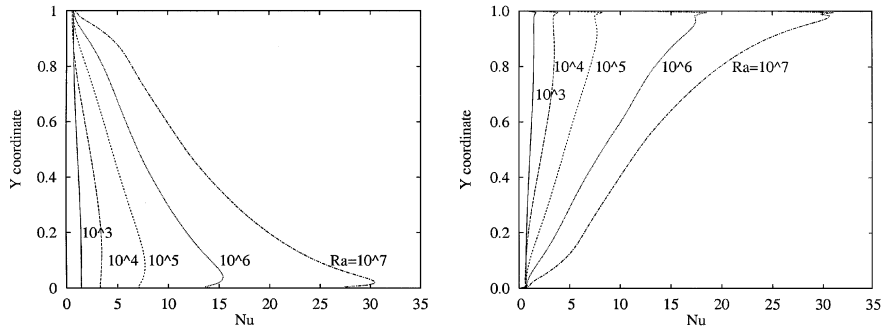


Figure 10. Natural convection cavity: Nusselt number along the hot (left) and cold (right) walls

Ra	10^3	10^4	10^5	10^6	10^7
$u_{1max}(y)$	3.68 (0.817)	16.1 (0.817)	34.0 (0.857)	6.54 (0.875)	139.7 (0.919)
de Vahl Davis (1983)	3.65 (0.813)	16.2 (0.823)	34.73 (0.855)	64.3 (0.850)	
$u_{2max}(y)$	3.73 (0.1827)	19.9 (0.1246)	70.0 (0.068)	228 (0.039)	698 (0.235)
de Vahl Davis (1983)	3.70 (0.178)	19.62 (0.119)	68.6 (0.066)	219.36 (0.038)	
Ramasawamy <i>et al.</i> (1992)		19.62	68.6	233	717
$Nu_{min}(y)$	0.623 (1)	0.4968 (1)	0.614 (1)	0.716 (1)	0.787 (1)
de Vahl Davis (1983)	0.692 (1)	0.586 (1)	0.729 (1)	0.989 (1)	
$Nu_{max}(y)$	1.47 (0.109)	3.47 (0.125)	7.71 (0.08)	17.46 (0.039)	30.46 (0.0236)
de Vahl Davis (1983)	1.50 (0.092)	3.53 (0.143)	7.71 (0.08)	17.92 (0.038)	
Ramasawamy <i>et al.</i> (1992)		3.5	7.71	17.0	30.0
$Nu_{1/2}$	1.1	2.33	4.49	8.24	11.76
de Vahl Davis (1983)	1.12	2.243	4.52	8.8	
Nu_{ave}	1.074	2.084	4.30	8.743	13.99
de Vahl Davis (1983)	1.12	2.243	4.52	8.8	

Table I. Comparison with the benchmark solution

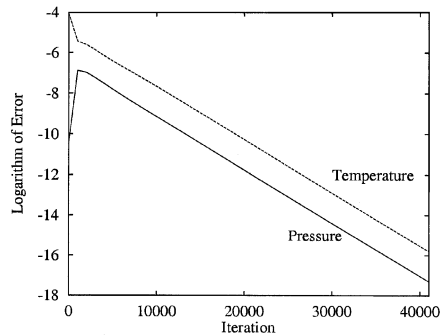


Figure 11. Natural convection in cavity: convergence history for pressure and temperature

Forced convection on tube bundle

The final test case is a forced convection over a tube bundle (Massarotti *et al.*, 1998). This type of flow is of practical importance in the heat exchanger industry. The tube bundle geometry is shown in Figure 12 where a staggered arrangement of both the relative longitudinal (a/d) and the transverse (b/d) pitches equal to 1.3 are used. Using the advantage of symmetric flow, the

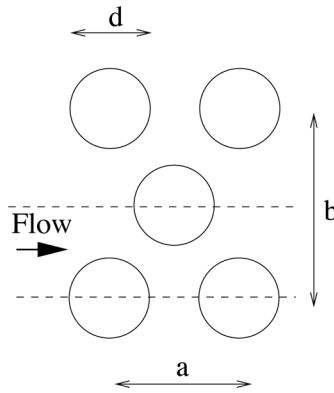
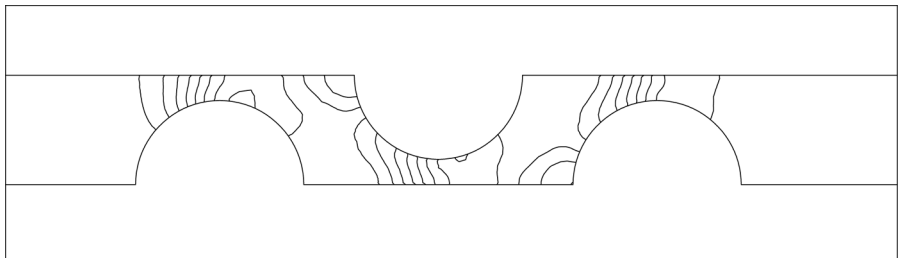
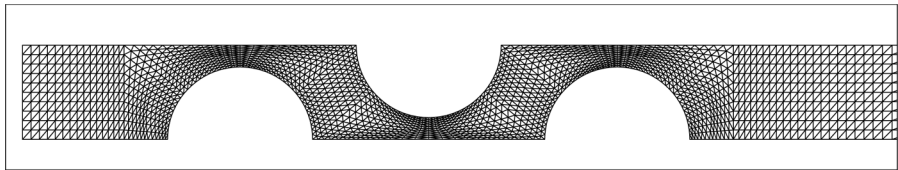
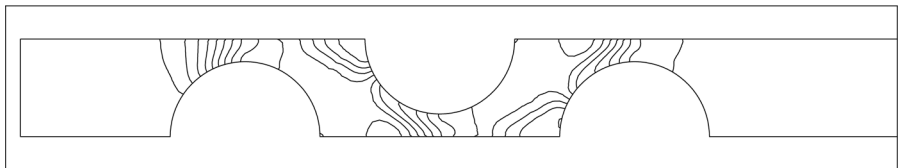


Figure 12. Forced convection on tube bundle: schematic of the problem (top) and part of the mesh used (bottom)



$Re = 50$



$Re = 150$

Figure 13. Forced convection on tube bundle: pressure contour plots

problem is only solved for the region between the two dashed lines shown in Figure 12. The problem is solved for two Reynolds numbers, i.e. $Re = 50$ and 150 and the Prandtl number is 1.0. The mesh used for this problem is partially shown in Figure 12 and consists of 3,948 triangular elements and 2,162 nodes. The flow domain downstream of the tube bundle is extended for as much as 15

An explicit finite element algorithm

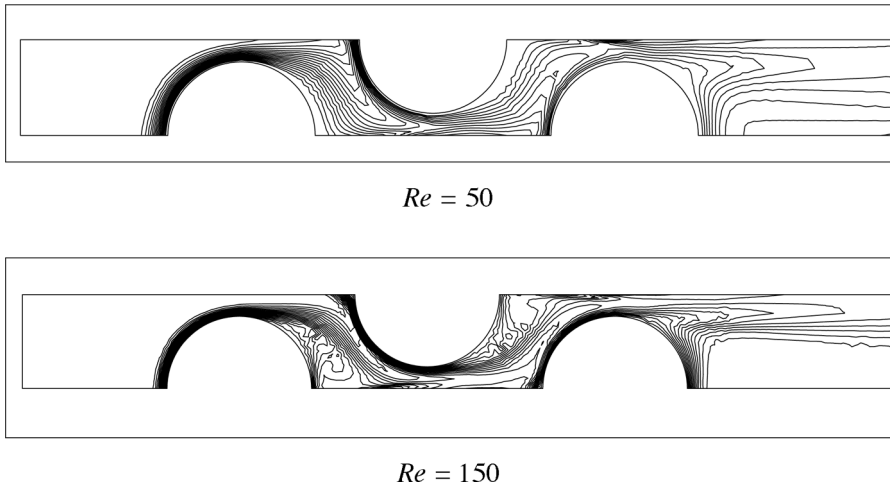


Figure 14. Forced convection on tube bundle: temperature contour plots

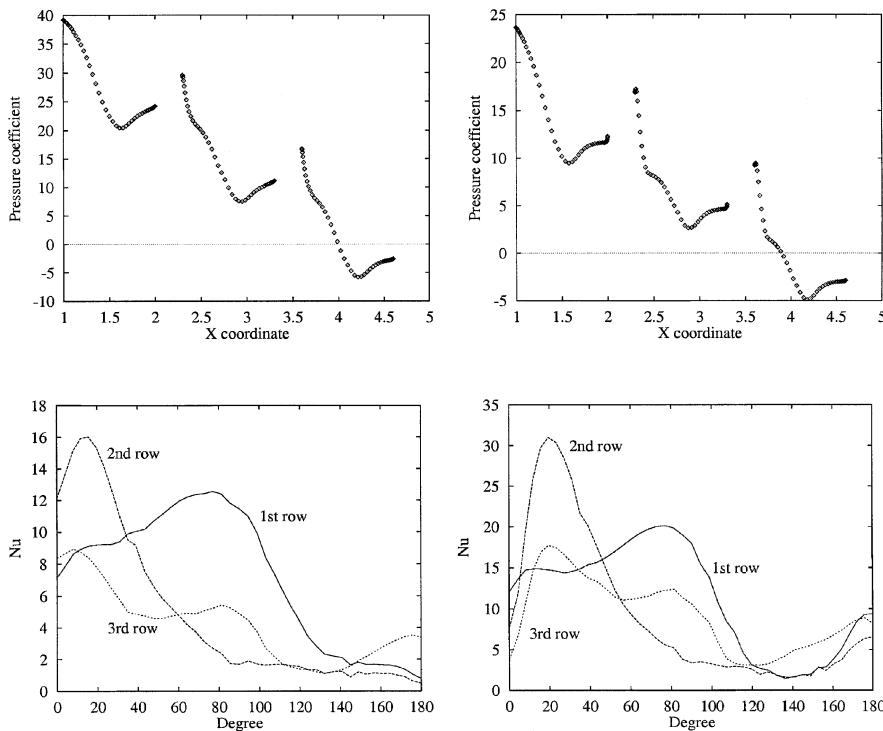


Figure 15. Forced convection on tube bundle: pressure distribution on the tubes (left: $Re = 50$, right $Re = 150$)

Figure 16. Forced convection on tube bundle: Nusselt number distribution on the tubes (left: $Re = 50$, right: $Re = 150$)

times the tube diameter for $Re = 50$ and 40 times for $Re = 150$. Figures 13 and 14 show the pressure and temperature contour plots for both Reynolds numbers. It is seen that very smooth results are obtained for both low and high Reynolds flows. In Figures 15 and 16, the pressure and Nusselt number distributions on the tubes are also illustrated.

Conclusions

It is shown that the incompressible flow with heat transfer can be accurately simulated using the proposed algorithm. It is also demonstrated that the method works well for both natural and forced convection problems. As an explicit time-stepping method is used, for certain flow conditions, a stable computation would require small time steps. However, even for such cases the total cpu time remains in a reasonable and affordable range and convergence to the steady state is fast. The practical convenience of the method will be more apparent when it is applied to the 3D problems. This is the subject of the author's current research.

References

- Armaly, B.F., Durst, F., Pereira, J.C.F. and Schönung, B. (1983), "Experimental and theoretical investigation of backward-facing step flow", *J. Fluid Mech.*, Vol. 127, pp. 473-96.
- Chorin, A.J. (1967), "A numerical method for solving incompressible viscous flow problems", *J. Comp. Physics*, Vol. 2, pp. 12-26.
- Denham, M.K. and Patrick, M.A. (1974), "Laminar flow over a downstream-facing step in a two-dimensional flow channel", *Trans. Inst. Chem. Engrs*, Vol. 52, pp. 361-7.
- de Vahl Davis, G. (1983), "Natural convection of air in a square cavity: a bench mark numerical solution", *Int. J. Numer. Methods in Fluids*, Vol. 3, pp. 249-64.
- Ghia, U., Ghia, K.N. and Shin, C.T. (1982), "High- Re solutions for incompressible flow using the Navier-Stokes equations and a multigrid method", *J. Comp. Phys.*, Vol. 48, pp. 387-411.
- Jameson, A., Schmidt, W. and Turkel, E. (1981), "Numerical simulation of the Euler equations by the finite volume method using Runge-Kutta time stepping schemes", AIAA Paper 81-1259.
- Lin, F.B. and Sotiropoulos, F. (1997), "Assessment of artificial dissipation models for three-dimensional incompressible flow solutions", *J. Fluids Engineering-Trans. ASME*, Vol. 119 No. 2, pp. 331-40.
- Lyra, P.R.M., Manzari, M.T., Morgan, K., Hassan, O. and Peraire, J. (1995), "Upwind side-based unstructured grid algorithms for compressible viscous flow computations", *Int. J. Eng. Anal. Des.*, Vol. 2, pp. 197-211.
- Manzari, M.T., Hassan, O., Morgan, K. and Weatherhill, N.P. (1998), "Turbulent flow computations on 3D unstructured grids", *Finite Elements in Analysis and Design*, Vol. 390, pp. 353-63.
- Massarotti, N., Nithiarasu, P. and Zienkiewicz, O.C. (1998), "Characteristic-based-split (CBS) algorithm for incompressible flow problems with heat transfer", *Int. J. Numer. Methods Heat & Fluid Flow*, Vol. 8 No. 8, pp. 969-90.
- Peraire, J., Peiró, J. and Morgan, K. (1993), "Multigrid solution of the 3-D compressible Euler equations on unstructured tetrahedral grids", *Int. J. Numer. Methods Eng.*, Vol. 36 No. 6, pp. 1029-44.

-
- Ramaswamy, B., Jue, T.C. and Akin, J.E. (1992), "Semi-implicit and explicit finite element scheme for coupled fluid/thermal problems", *Int. J. Numer. Methods Eng.*, Vol. 34, pp. 675-96.
- Rizzi, A. and Eriksson, L.E. (1984), "Computation of flow around wings based on the Euler equations", *J. Fluid Mech.*, Vol. 148, pp. 45-71.
- Tamamidis, P., Zhang, G.Q. and Assanis, D.N. (1996), "Comparison of pressure-based and artificial compressibility methods for solving 3D steady incompressible viscous flows", *J. Comp. Phys.*, Vol. 124 No. 1, pp. 1-13.
- Wasfy, T., West, A.C. and Modi, V. (1998), "Parallel finite element computation of unsteady incompressible flows", *Int. J. Numer. Methods in Fluids*, Vol. 26, pp. 17-36.